THE JOURNAL OF BIOLOGICAL CHEMISTRY VOL. 287, NO. 26, pp. 22387–22396, June 22, 2012

Rigidity of Wedge Loop in PACSIN 3 Protein Is a Key Factor in Dictating Diameters of Tubules*[S]

Received for publication, March 4, 2012, and in revised form, April 26, 2012 Published, JBC Papers in Press, May 9, 2012, DOI 10.1074/jbc.M112.358960

Xiaoyun Bai[‡§1], **Geng Meng**[‡§1], **Ming Luo**[¶], **and Xiaofeng Zheng**[‡§2]

From the [‡]*State Key Laboratory of Protein and Plant Gene Research,* [§]*Department of Biochemistry and Molecular Biology, School of Life Sciences, Peking University, Beijing 100871, China and the* [¶]*Department of Microbiology, University of Alabama at Birmingham, Birmingham, Alabama 35294*

Background: PACSINs participate in cellular membrane remodeling.
Results: PACSIN 3 F-BAR induces different tubules compared with PACSIN 1 and 2. Structures of PACSINs reveal a novel wedge loop-mediated lateral interaction and different packing mode in PACSIN 3.
Conclusion: The rigidity of the wedge loop determines the angles between neighboring dimers and further dictates tubule diameters.
Significance: The study provides novel insights into F-BAR domain-induced membrane deformation.

BAR (Bin/amphiphysin/Rvs) domain-containing proteins participate in cellular membrane remodeling. The F-BAR proteins normally generate low curvature tubules. However, in the PACSIN subfamily, the F-BAR domain from PACSIN 1 and 2 can induce both high and low curvature tubules. We found that unlike PACSIN 1 and 2, PACSIN 3 could only induce low curvature tubules. To elucidate the key factors that dictate the tubule curvature, crystal structures of all three PACSIN F-BAR domains were determined. A novel type of lateral interaction mediated by a wedge loop is observed between the F-BAR neighboring dimers. Comparisons of the structures of PACSIN 3 with PACSIN 1 and 2 indicate that the wedge loop of PACSIN 3 is more rigid, which influences the lateral interactions between assembled dimers. We further identified the residues that affect the rigidity of the loop by mutagenesis and determined the structures of two PACSIN 3 wedge loop mutants. Our results suggest that the rigidity-mediated conformations of the wedge loop correlate well with the various crystal packing modes and membrane tubulations. Thus, the rigidity of the wedge loop is a key factor in dictating tubule diameters.

Cellular membrane deformation is important in the process of cargo transportation and cell movement (1–5). Membrane remodeling is induced by the packing of protein oligomers on the negatively charged membrane surface (6–8). The Bin/amphiphysin/Rvs (BAR)[3] domain proteins, including N-BAR (N-terminal amphipathic helix-BAR), EFC/F-BAR (Fes/CIP4 homology-BAR), and IMD/IBAR (inverse-BAR) domain proteins, are important for membrane remodeling in vesicle budding, membrane trafficking between intracellular compartments, and cell division (6, 9–14). F-BAR domain proteins contain a central α-helix bundle that stabilizes the membrane via the positively charged protein surface of homodimer and bends the membrane into tubules with low curvature (8, 15–17). The crystal structures of FBP17 and CIP4 revealed that F-BAR domain proteins form filaments through end-to-end interactions between dimers in the crystal, and the diameters of the induced tubules were proposed to be related to the intrinsic large radial curvature of the F-BAR dimer (16). Cryo-EM studies of CIP4 and FBP17 showed that the F-BAR domain-induced membrane tubulation is caused by the packing of the protein helical lattice on the membrane surface via lateral and tip-to-tip interactions of the F-BAR dimers (18).

PACSINs (also named syndapin) constitute a branch of the F-BAR domain protein family, which are cytoplasmic proteins involved in receptor-mediated endocytosis, synaptic vesicle trafficking, and biogenesis of different cellular organelles (11, 19–26). PACSINs contain the N-terminal F-BAR domain and a C-terminal mono-Src homology 3 domain. The PACSIN family contains PACSIN 1, 2, and 3, which differ in their tissue distributions. PACSIN 1 is detected primarily in neuron cells, and PACSIN 3 is found in lung and muscle tissues, whereas PACSIN 2 is expressed ubiquitously (21, 27, 28). The F-BAR-mediated membrane deformation of PACSIN 1 is autoinhibited by its Src homology 3 domain (29). Interactions of PACSINs with other proteins such as dynamin and the neutal Wiskott-Aldrich syndrome protein also play important roles in membrane remodeling activities (30).

In contrast to the typical F-BAR domain proteins that mainly generate low curvature tubules (100 nm in diameter), PACSIN

* This work was supported by National High Technology and Development Program of China Grant 2010CB911804, National Science Foundation of China Grant 30930020, and International Centre for Genetic Engineering and Biotechnology Project CRP/CHN09-01.
[S] This article contains supplemental Figs. S1–S7.
The atomic coordinates and structure factors (codes 3Q84, 3Q0K, 3QE6, 3M3W, and 3SYV) have been deposited in the Protein Data Bank, Research Collaboratory for Structural Bioinformatics, Rutgers University, New Brunswick, NJ (http://www.rcsb.org/).
[1] Both authors contributed equally to this work.
[2] To whom correspondence should be addressed: School of Life Sciences, Peking University, Beijing, 100871 China. Tel.: 86-10-6275-5712; Fax: 86-10-6276-5913; E-mail: xiaofengz@pku.edu.cn.

[3] The abbreviations used are: BAR protein, Bin/amphiphysin/Rvs domain protein; PACSIN, protein kinase C and casein kinase substrate in neurons protein; PDB, Protein Data Bank.

1 and 2 can induce a wide range radius of membrane tubules including not only the typical 100-nm tubule but also smaller tubules with an average diameter of 10 nm. In addition, they also facilitate tubule constrictions (31). Both crystal structures of the F-BAR domain of PACSIN 1 and 2 reveal a unique wedge loop, which was proposed to contribute to membrane insertion and binding (31). A hinge in the distal end of the murine PACSIN 2 F-BAR domain was predicted to contribute to membrane curvature sensing (32). However, the detailed mechanism of how the F-BAR dimers of PACSIN induce various curvature tubulations remains unclear.

To elucidate further the mechanism of membrane remodeling by the F-BAR domain of PACSINs, we investigated the membrane deformation by the PACSIN 3 F-BAR domain compared with PACSIN 1 and PACSIN 2 F-BAR domains, by negative-stain electron microscopy. We further determined the structures of the F-BAR domains from PACSIN 3, PACSIN 1, PACSIN 2, and two PACSIN 3 loop mutants, E128A and P121Q. We found that different from PACSIN 1 and 2, PACSIN 3 could only induce ~100-nm tubules. Based on structure studies, we discovered that the more rigid PACSIN 3 wedge loop, which is in a different structural conformation compared with PACSIN 1 and 2, contributes to the distinct lattice formed by the PACSIN 3 F-BAR domain in the crystal. The parallel lattice of PACSIN 3 reveals a novel type of wedge loop-mediated lateral interaction between neighboring dimers, and the lattice is related to protein packing on the tubulated membrane. We further identified the residues that determine the rigidity of the wedge loop in the PACSIN 3 F-BAR domain. The mutations of these residues change the structural conformation of the wedge loop, which alters the wedge loop-mediated lateral interactions between neighboring dimers and further influences the membrane curvature. Therefore, the rigidity of the wedge loop in PACSIN 3 is a key factor in dictating the diameters of tubules.

EXPERIMENTAL PROCEDURES

Protein Expression and Purification—The F-BAR domain of PACSIN 1 (residues 1–344), PACSIN 1 mutants, the F-BAR domain of PACSIN 2 (residues 1–372) and PACSIN 2 mutant E130A, the F-BAR domain of mouse PACSIN 3 (residues 1–341, which has 94% amino acid sequence identity to human PACSIN 3) and PACSIN 3 mutants, were cloned into pET28a vector. All proteins except PACSIN 1 truncate 1–344 were expressed in *Escherichia coli* BL21 (DE3) cells and purified on a Ni^{2+}-HiTrap affinity column followed by a Superdex-75 column (GE Healthcare) (33).

PACSIN 1 truncate 1–344 was expressed in B834 cells which were cultured in M9 minimal medium supplemented with 50 mg/liter kanamycin and 40 mg/liter selenomethionine, and purified as described (33).

Protein Crystallization and Structural Determination—Initial crystallization conditions were screened using kits from Hampton Research including PEG, Crystal Screen, Crystal Screen 2, and Index. Crystals were optimized by the hanging-drop vapor diffusion method. Drops were prepared by mixing 2 μl of protein solution (8 mg/ml protein in 500 mM NaCl, 10 mM HEPES, pH 7.5) with 2 μl of reservoir solution and were equilibrated against 500 μl of reservoir solution at 293 K. A large crystal of PACSIN 1 F-BAR (600 × 190 × 200 μm) was obtained within 2 weeks from 200 mM $NH_4H_2PO_4$, 100 mM HEPES, pH 7.5, 16% PEG 3350 (w/v), and 5% glycerol. The crystal of PACSIN 2 F-BAR was obtained from 100 mM $MgCl_2$, 100 mM sodium cacodylate, pH 6.5, 18% PEG 3350 (w/v) within 2 days. The crystal of PACSIN 3 F-BAR was obtained from 200 mM KSCN, 100 mM HEPES, pH 7.3, 100 mM $CaCl_2$, 20% PEG 3350 (w/v) within 3 days. The crystal of PACSIN 3 E128A was obtained from 200 mM CH_3COONH_4, 100 mM $CaCl_2$, 16% PEG 3350 (w/v), and PACSIN 3 P121Q from 0.5 M ammonium sulfate, 0.1 M sodium citrate tribasic dehydrate, pH 5.6, 1.0 M lithium sulfate monohydrate within 10 days. 15, 15, 25, 20, and 28% glycerol was used as cryoprotectant for PACSIN 1, PACSIN 2, PACSIN 3, PACSIN 3 E128A, and PACSIN 3 P121Q.

For crystal data collection, crystals were flash-cooled with a nitrogen stream at 100 K, and x-ray diffraction data were collected on Mar 345 image plate detector at SSRF. Data of PACSIN 1(1–344) were processed with HKL2000 and MLPHARE software (34). Images of the F-BAR domains of PACSIN 1, PACSIN 2, PACSIN 3, PACSIN 3 mutant E128A, and PACSIN 3 P121Q were integrated with Mosflm (35), and data were carried out by Molecular Replacement by CCP4 (34) with PACSIN 1–344 as the model, and finally refined by COOT (36).

Liposome Preparation—Lipids containing 80% DOPC and 20% DOPA (Avanti) were mixed and dissolved in chloroform. The organic solvent was removed by evaporation under a stream of nitrogen gas, followed by incubation for 2 h in a vacuum to ensure complete removal of solvent. Lipid films were resuspended in HEPES buffer (10 mM HEPES, pH 7.4, 50 mM NaCl, 0.2 mM EDTA) and subjected to 10 freeze-thaw cycles. Large unilamellar vesicles were then formed by extrusion through 100-nm nucleopore polycarbonate membranes. The prepared liposomes were stored at 4 °C.

Liposome Sedimentation Assay—Protein (1 mg/ml) was incubated with liposome (1 mg/ml) with 1:1 protein-lipid volume ratio for 20 min at room temperature. The protein-lipid mixture was centrifuged at 140,000 × *g* for 30 min at 4 °C in an ultracentrifuge (Beckman TLA100 rotor). Supernatants were then collected, and pellets were resuspended in 40 μl of sample buffer. Proteins in both fractions were subjected to SDS-PAGE, stained with Coomassie Blue, and visualized by a Bio-Rad XRS system.

Tubulation Assays—Protein (1 mg/ml) was incubated with liposome (1 mg/ml) with 1:1 protein-lipid volume ratio for 5 min at room temperature. 6-μl protein-liposome samples were then spread onto freshly glow-discharged Formvar- and carbon-coated electron microscopy grids, stained with 2% uranyl acetate for 1 min, and air dried at room temperature. The grid was examined on a transmission electron microscope (FEI 200 kV) with the electron energy set to 120 kV.

Nanogold Labeling Tubulation Assays—Protein (1 mg/ml) was incubated with liposome (1 mg/ml) with 1:1 protein-lipid volume ratio for 5 min at room temperature. 6-μl protein-liposome samples were then spread onto freshly glow-discharged Formvar- and carbon-coated electron microscopy grids and stained with 5 nm Ni-nitrilotriacetic acid-nanogold (Nanoprobes) for 1 min at room temperature followed by staining with 2% uranyl acetate for 1 min and air dried at room temper-

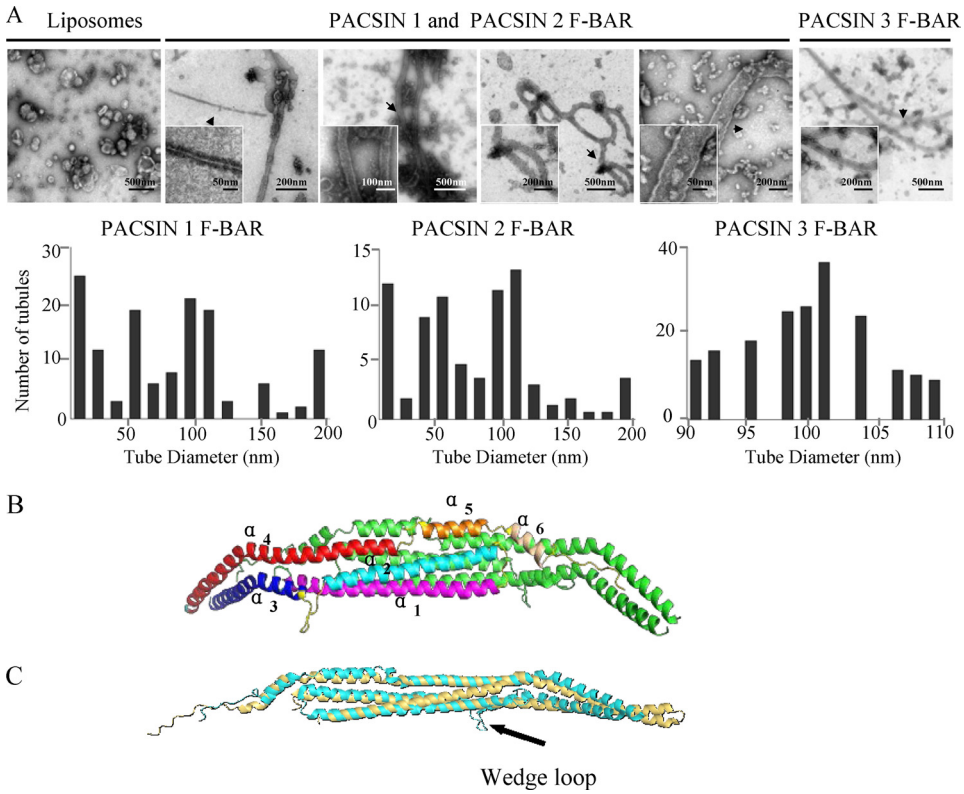

FIGURE 1. **PACSIN-induced liposome tubulation.** *A*, negative stain EM images of liposomes and tubules induced by PACSIN 3 and PACSIN 1, two F-BAR domains, and quantification of liposome tubulation in the same experiment. Liposomes were incubated with the purified F-BAR domain of PACSIN 1 (residues 1–344), PACSIN 2 (residues 1–372), and PACSIN 3 (residues 1–341). *Insets* show the higher magnifications of the tubules indicated by *arrows*. *Scale bars*, 50, 100, and 500 nm, respectively. *B*, ribbon presentation of the F-BAR dimers of PASCIN 3. The two monomers interact with each other in an antiparallel manner. Each monomer consists of six α-helices named 1–6. One monomer is tinted in a different color for the six α-helices; the other is colored in *green*. *C*, superimposition of the F-BAR domain between PACSIN 3 (Protein Data Bank (PDB) code 3QE6) and FBP17 (PDB code 2EFL). Ribbon representation is shown. PACSIN 3 and FBP17 are colored in *cyan* and *yellow*, respectively. The *arrow* indicates the unique wedge loop in the PACSIN family proteins that is not found in any other F-BAR domain structure.

ature. The grid was examined on a transmission electron microscope (FEI 200 kV) with electron energy set to 120 kV.

RESULTS

Membrane Tubulation Induced by F-BAR Domain of PACSIN 3 Is Different from PACSIN 1 and 2—To investigate the membrane deformation induced by PACSINs, the F-BAR domains from PACSIN 1, 2, and PACSIN 3 were expressed in *E. coli* and purified to near homogeneity. Liposome tubulation induced by F-BAR domains was examined by negative stain electron microscopy. Unlike other F-BAR domain-containing proteins, tubules induced by PACSIN 1 and 2 have various diameters, which is consistent with previous reports (31). These tubules are mainly classified into three classes: the first class has low curvature with a diameter of ~100 nm, the second class has intermediate curvature with a diameter of ~50 nm, and the third class has high curvature with a diameter of ~10 nm (Fig. 1*A*). In addition, tubules with other diameters were also observed. In contrast, the PACSIN 3 F-BAR domain could only induce low curvature tubules of ~100-nm diameter (Fig. 1*A*), despite sharing 55 and 60% sequence identity with the F-BAR domain of PACSIN 1 and 2, respectively.

Crystal Structure of PACSIN 3 F-BAR Domain Shows Novel Type of Lateral Interaction Mediated by Wedge Loop—To elucidate the molecular mechanism to explain the differences in membrane tubulation between PACSIN 3 and PACSIN 1, 2, we crystallized and determined the structures of the F-BAR domain of PACSIN 3 (residues 1–304), as well as that of PACSIN 1 (residues 14–308) and PACSIN 2 (residues 1–304) (supplemental Fig. 1 and Table 1). The structure of the PACSIN 1 F-BAR domain was determined by single anomalous dispersion phasing, using data collected with a crystal of selenomethionine-derivatized protein, and the structures of PACSIN 2 and PACSIN 3 F-BAR domains were solved by molecular replacement using the initial structure of the PACSIN 1 F-BAR domain as the searching model. The structures of PACSIN 1, PACSIN 2, and PACSIN 3 F-BAR domains were refined to resolutions of 2.9, 2.7, and 2.6 Å in the space groups C2, $P2_1$, and $P2_1$, respectively (Table 1). The structures showed that PACSINs form a dimer in the crystal and adopt a crescent shape with a six-helix bundle core and two three-helix bundle arms extending from the central body. Each monomer is composed of six α-helices that interact with the other monomer in an antiparallel manner. Two neighboring helices α1 form the main central dimerization interface that are flanked by two wings composed of helix α3 and the curved region of helix α4. Helix α3 and a longer helix α4 both extend the length of the monomer with bending ends. Helix α2 and the shorter helices α5 and α6 generate the bundle center that is associated with helix α1 (Fig. 1*B*

TABLE 1
Data collection and refinement statistics

	Se-PACSIN (residues 1–307)	PACSIN 2 (residues 1–304)	PACSIN 3 (residues 1–304)	PACSIN3E128A (residues 1–302)	PACSIN3P121Q (residues 6–299)
Diffraction data					
Space group	C2	$P2_1$	$P2_1$	$P2_1$	$P2_1$
Unit cell parameters					
(*a*, *b*, *c*) (Å)	85.3, 154.3, 215.4	31.58, 86.13, 353.80	46.9, 54.7, 193.7	47.5, 52.3, 196.5	120.570, 108.901, 222.319
$\alpha\beta\gamma$	90, 90.3, 90	90, 90, 90	90, 96.9, 90	90, 94.8, 90	90.00, 90.05, 90.00
Resolution range (Å)	30–2.8 (2.91–2.8)	30–2.6 (2.75–2.6)	30–2.6 (2.67–2.6)	15–2.6 (2.67–2.6)	50–3.1 (3.18–3.1)
Unique reflections	63,353	41,646	28,175	28,283	98,202
Completeness (%)	96.2 (87.43)	99.7 (85.9)	97.8 (90.8)	99.8 (93.7)	98.68 (98.02)
Mean $I/\sigma(I)$	16.65 (2.5)	14.5 (2.5)	35.4 (3.4)	14.2 (2.4)	18.3 (3.1)
Multiplicity	4.3	3.1	4.1	4	4.3
Refinement					
R_{work}/R_{free} (%)[a]	22.1/29.4	20.77/29.2	22.7/27.4	23.2/28.1	27/33.6
Modeled chain: residues A					
Non-H atoms (protein/water)	13,874/213	9,683//202	4,648/34	4,587/10	16,535/197
Root mean square deviations					
Bonds (Å)/Angles (°)	0.017/1.692	0.015/1.593	0.022/2.041	0.011/1.297	0.0213/2.009
Ramachandran analysis					
Favored	98.61	98.14	93.94	96.22	94.01
Allowed	1.33	1.68	5.81	3.78	5.14
Generously allowed	0.06	0.18	0.24	0	0.86
Disallowed	0	0	0	0	0

[a] $R = \Sigma||F_o| - |F_c||/\Sigma|F_o|$. The full-length PACSINs proteins were first crystallized but degraded from the C-terminal Src homology 3 domain. Then the truncation of Se-PACSIN (residues 1–305), PACSIN 2 (residues 1–305), and PACSIN 3 (residues 1–302) was designed and crystallized.

and supplemental Fig. 1*A*). The structure-based sequence alignment of the residues on the protein surface of the F-BAR domains of PACSINs showed that the positively charged residues on the concave surface are highly conserved (supplemental Fig. 1, *B* and *C*). Consistent with the previously determined structures of the F-BAR domain of PACSIN 1 and 2 (31), the wedge loop between helices α2 and α3 is also present in PACSIN 3, which is a distinct feature of the F-BAR domain of PACSINs and has not been observed in other BAR domain-containing families (Fig. 1*C*).

Despite the structure similarity between the F-BAR dimer of PACSIN 3 and those of PACSIN 1 and 2, we found that the packing patterns of the neighboring dimers of these proteins are strikingly different in the crystal: PACSIN 3 shows only a parallel packing among all the different crystallization conditions that have been examined, whereas PACSIN 1 and 2 show different packing modes (supplemental Fig. 2).

We also found that the parallel packing of the PACSIN 3 F-BAR domain is similar to the packing lattice of the CIP4 F-BAR domain observed on the tubules by cryo-EM (18). However, a close-up view of the PACSIN 3 structure reveals a distinct type of lateral interaction between two neighboring dimers (Fig. 2*A*), in addition to the typical CIP4-like tip-to-tip interaction. In CIP4, the lateral interactions between the neighboring dimers involve only the residues of neighboring helices, whereas in PACSIN 3, the lateral interactions are between one of the PACSIN-specific wedge loops with the helix α2 of the neighboring dimer (Fig. 2, *A*, *left*, and *B*, *upper*). The other wedge loop of the same dimer extends out into the membrane direction (Fig. 2, *A*, *right*, and *B*, *lower*). This observation suggests that the wedge loop might function in two ways: one loop in the dimer is involved in the lateral interaction, and the other loop in the dimer extends out and inserts into the membrane bilayer.

Dual Roles of Wedge Loop in Mediating Protein Packing and Membrane Binding—To confirm that the wedge loop is involved in the interactions between the neighboring dimers, we mutated the residues located in the lateral contacting area (Fig. 2*C*, *left*). A total of 15 mutants of the five residues on the contacting surface were constructed. The mutants were purified and examined by a liposome tubulation assay (Fig. 3*A*). The binding of these mutants to liposomes was investigated by a sedimentation assay (Fig. 3*B*). Mutations in the wedge loop (H119E/A/Q, R127E/A/Q) or in the contacting area (E93R/A/Q, E97R/A/Q and E100R/A/Q) abolished the liposome tubulation activity completely, but retained the liposome binding ability (Fig. 3 and supplemental Fig. 3*B*). This observation indicates that the interaction between the wedge loop and its neighboring dimer plays critical roles in protein packing on the membrane to induce liposome tubulation.

We further examined the residues on the wedge loop that may insert into the membrane bilayer. A series of mutants of the wedge loop, ΔV122L123, V122E/L123E, and V122R/L123R of PACSIN 3 (Fig. 2*C*, *right*) were constructed in which the two bulky hydrophobic residues at the base of the wedge loop were either deleted or mutated. The liposome tubulation activities and the binding of these mutants to liposomes were also investigated. Our results showed that the deletion of the wedge loop (ΔV122L123) or mutation of residues Val-122 and Leu-123 at the center of the wedge loop to Glu or Arg (V122E/L123E, V122R/L123R) totally abolished induction of tubules and reduced liposome binding (Fig. 3*B*), which is consistent with the observation in the site mutation constructs I125E or M126E previously reported in PACSIN 1 (31). These results indicate that the wedge loop binds liposomes through hydrophobic residues Val-122 and Leu-123 (or Ile-125/Met-126 in PACSIN 1, and Met-124/Met-125 in PACSIN 2, supplemental Fig. 3*B*).

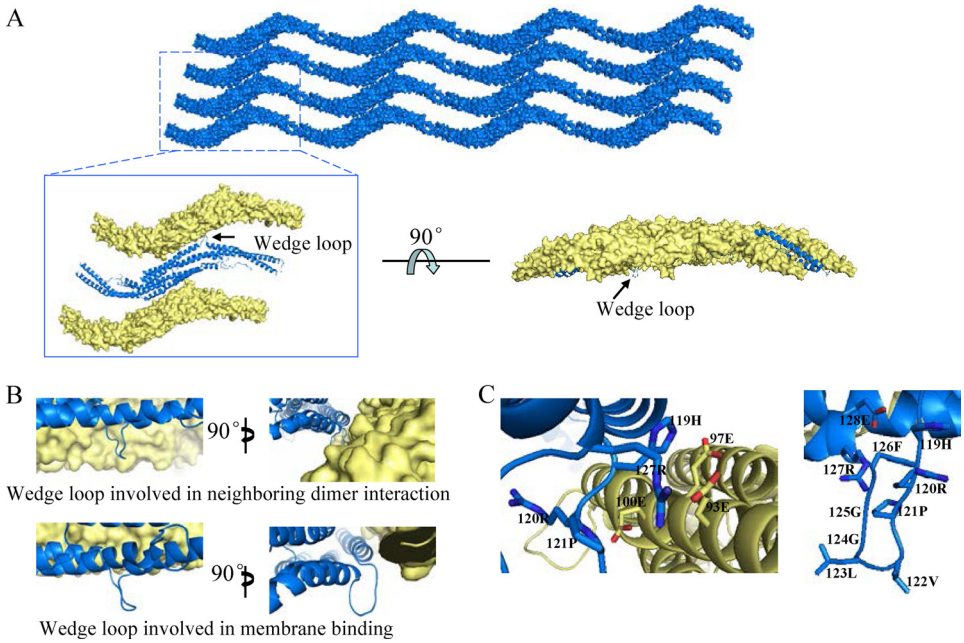

FIGURE 2. **Wedge loop plays dual roles in PACSIN 3 packing.** *A*, novel type of loop-mediated lateral interaction found in PACSIN 3 F-BAR packing. The PACSIN 3 F-BAR domain packs in a parallel manner which connected by tip-to-tip interactions and the loop-mediated lateral interactions. *B*, close-up view of the two wedge loops in the same dimer. One of the wedge loops interacts with its adjacent dimer (*upper*). The other wedge loop is exposed and extrudes into the target membrane direction (*lower*). The *right view* is rotated by 90° clockwise relative to the *left view*. The two adjacent dimers are colored *marine* and *yellow*, and presented as ribbon and surface, respectively. *C*, *left image* showing residues on the contacting surface between the wedge loop and the neighboring dimer. Indicated residues are shown as side chain *sticks*. *Right image* shows the membrane binding wedge loop from residue His-119 to Glu-128 and is presented as side chain *sticks*.

There is a possibility that the mutant proteins may be distorted in structure, thus influencing the membrane tubulation property. We therefore monitored the secondary structure of all of the mutant proteins by a circular dichroism assay. Our results showed that the secondary structures of these mutants are similar to the wild-type protein (supplemental Fig. 3), indicating that the lost of the tubulation activity is caused by the elimination of protein-protein interaction, not by destroying the structure of the protein.

To characterize further where the PACSIN proteins localize in the tubulation process, 5-nm Ni^{2+}-nitrilotriacetic acid-linked nanogold particles were used to label the His-tagged PACSIN F-BAR proteins in tubulation assays (Fig. 3*C*). The results showed that the nanogold particles were concentrated on the surface of the tubules. This observation indicates that tubules are induced by the PACSIN F-BAR proteins.

Rigidity of Wedge Loop Influences Lateral Interactions and Dictates Diameter of Tubules—Superimposition of the wedge loops among PACSIN 3 and PACSIN 1 and 2 revealed that the wedge loop of PACSIN 3 has a different conformation. The wedge loop of PACSIN 3 is wider and bends more toward the inner side of the dimer compared with the relatively flat, outward-splayed loops in PACSIN 1 and 2 (Fig. 4*A*, *left*). We therefore hypothesized that the conformational difference of the wedge loops would be an important factor in determination of the interaction pattern between neighboring dimers and would contribute further to the variations in membrane tubulation.

Structure-based sequence alignments of the wedge loop region in PACSINs revealed that the predominant difference between PACSIN 3 and PACSIN 1 or 2 is residue Pro-121 located in the center of the wedge loop of PACSIN 3, which superimposes onto residue Gln-124 and Gln-123 in PACSIN 1 and 2, respectively (Fig. 4, *B* and *C*). The rigidity of the proline residue may restrain the flexibility of the wedge loop in PACSIN 3 and affect the interaction pattern between neighboring dimers and membrane tubulation.

To verify the above predictions, we mutated Pro-121 of PACSIN 3 to glutamine, which is found in PACSIN 1 and 2, and substituted the equivalent glutamine of PACSIN 1 and 2 with proline. The effects of the mutant proteins on liposome tubulation were investigated by negative stain EM. Consistent with the hypothesis, replacement of proline with glutamine at position 121 (P121Q) in PACSIN 3 led to the formation of a large number of pseudopod-like small tubules, in addition to the large tubules (Fig. 5*A*). These pseudopod-like tubules were approximately 10 nm in diameter, and some are budded from the surface of the large tubules. At the same time, replacement of Gln with Pro in PACSIN 1 Q124P and PACSIN 2 Q123P induced only one type of large tubules that are ~100-nm in diameter (Fig. 5*B*). Moreover, we determined the crystal structure of the PACSIN 3 P121Q mutant to 2.9 Å resolution (supplemental Fig. 4 and Table 1). The structure revealed that the mutation of proline to glutamine changed the orientation of the wedge loop of PACSIN 3, and the wedge loop in the mutant structure points outward and superimposes very well with the wedge loop of native PACSIN 1 and 2 (Fig. 4*A*, *middle*). In addition, the crystal packing of PACSIN 3 P121Q showed an obvious change of the angle between the neighboring dimers, which resembles that found in PACSIN 1 and 2 packing lattices (supplemental Fig. 2). These results demonstrate that the rigidity of the wedge loop in the PACSINs F-BAR domain correlates with the conformational change of the wedge loop and further

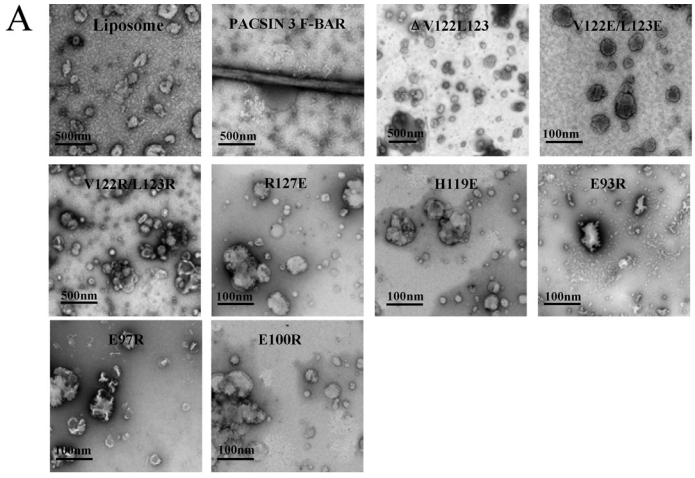
A
Liposome
PACSIN 3 F-BAR
ΔV122L123
V122E/L123E
V122R/L123R
R127E
H119E
E93R
E97R
E100R
500nm
100nm

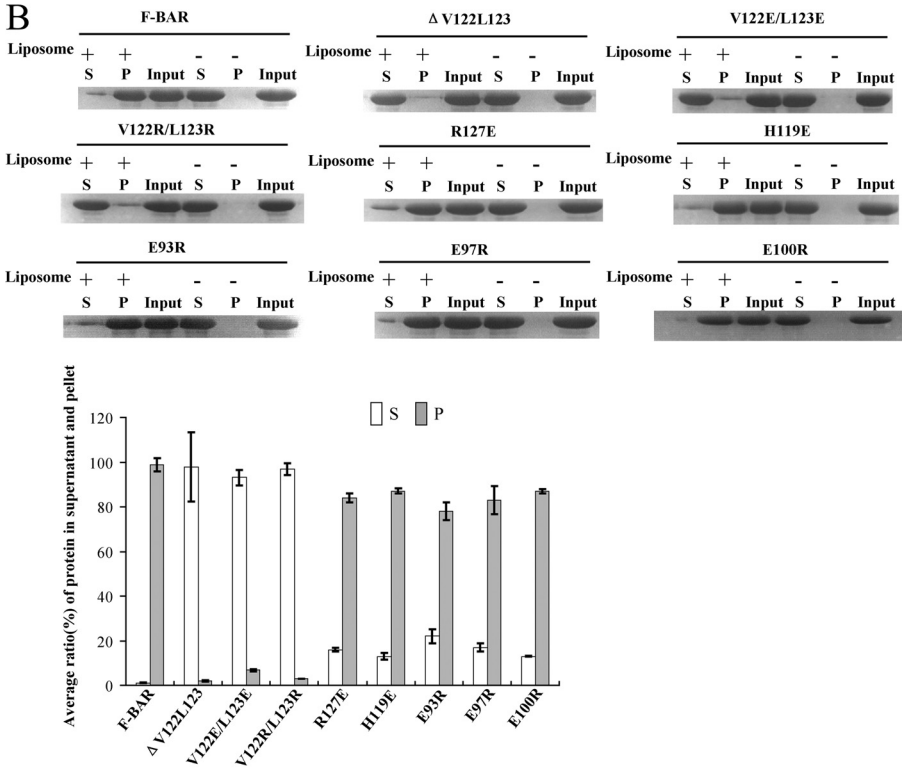
B
F-BAR
ΔV122L123
V122E/L123E
V122R/L123R
R127E
H119E
E93R
E97R
E100R
Liposome
S P Input S P Input
Average ratio(%) of protein in supernatant and pellet
S P
F-BAR
ΔV122L123
V122E/L123E
V122R/L123R
R127E
H119E
E93R
E97R
E100R

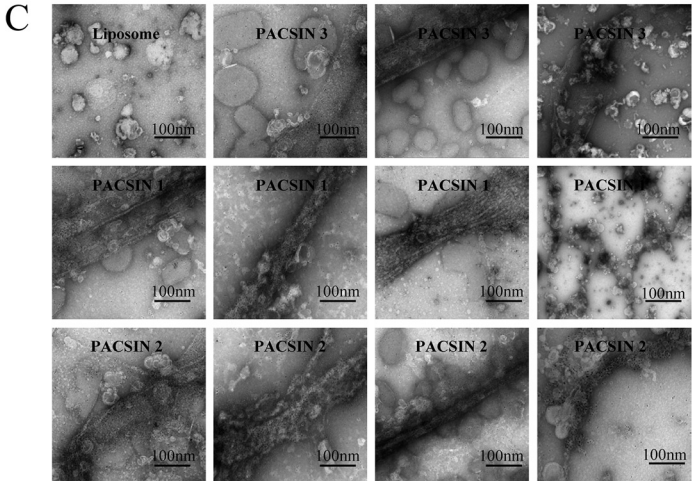
C
Liposome
PACSIN 3
PACSIN 1
PACSIN 2
100nm

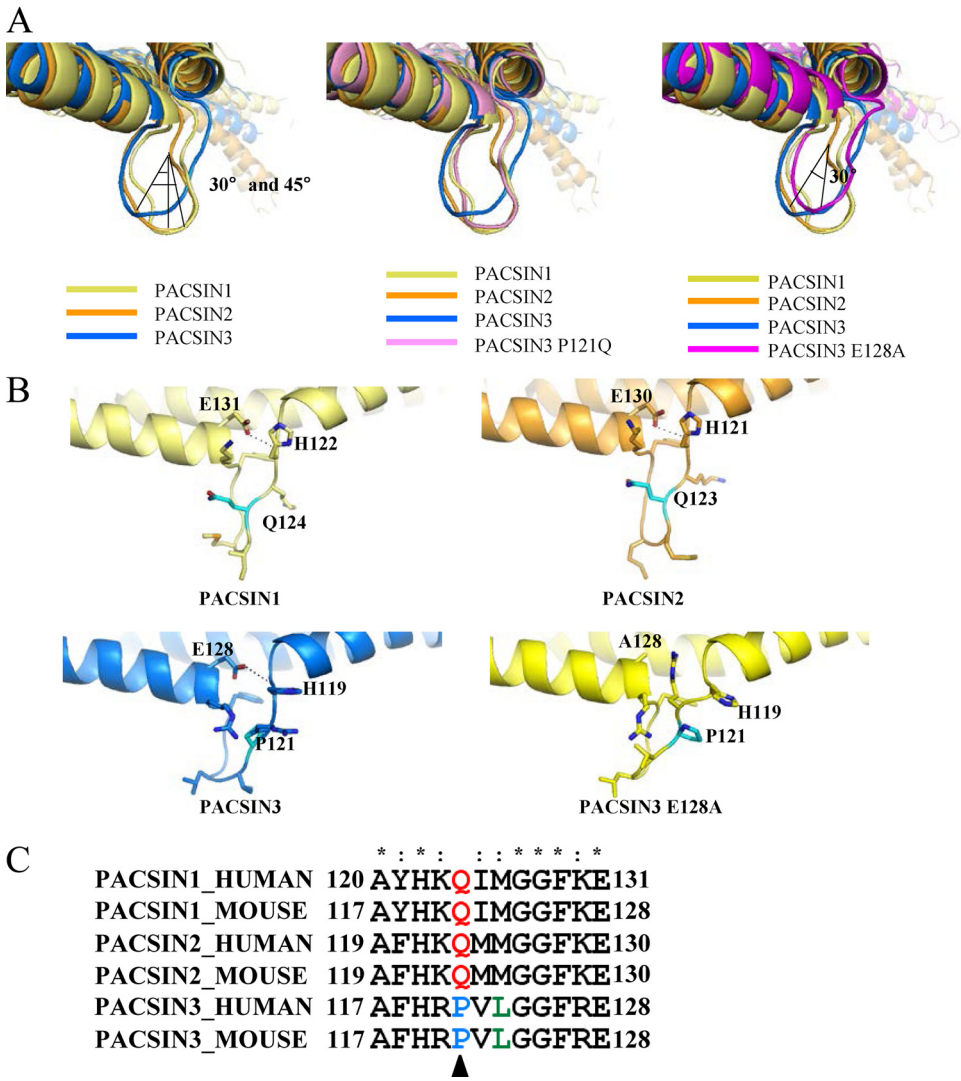

FIGURE 4. **Comparisons of the wedge loop among PACSINs.** *A*, structural alignments of the wedge loop among PACSIN 1, 2, 3 and PACSIN 3 mutants P121Q and E128A. The wedge loop in PACSIN 3 points inward by 45° compared with PACSIN 2 and points inward by 30° compared with PACSIN 1 (*left*). Compared with the wedge loop in the wild-type PACSIN 3 F-BAR domain, the wedge loop in the PACSIN 3 P121Q mutant swings outward and is superimposable with the wedge loop of PACSIN 1 and 2 (*middle*); and the wedge loop in the PACSIN3 E128A mutant reoriented significantly by swinging 30° outward to resemble the outward-splayed wedge loop in PACSIN 1 and PACSIN 2 (*right*). *B*, close-up view of the wedge loops of PACSIN 1, PACSIN 2, PACSIN 3, and PACSIN 3 E128A mutant. All of the native structures of the PACSIN F-BAR domains include a conserved hydrogen bond between Glu and His at the base of the wedge loop (Glu-131 and His-122 for PACSIN 1, Glu-130 and His-121 for PACSIN 2, and Glu-128 and His-119 for PACSIN 3), whereas this hydrogen bond is absent in the PACSIN 3 E128A mutant. *C*, sequence alignments of the wedge loop among PACSINs from human and mouse using ClustalX. Instead of the conserved residue Gln in PASCIN 1 and 2, it is a conformationally restrained Pro residue at position 121 in PACSIN 3. *Asterisks* and *colons* indicate homology sequence among PACSIN 1 PACSIN 2 and PACSIN 3.

affects lateral interactions of neighboring dimers and membrane tubulation.

To investigate whether mutation of Pro-121 in PACSIN 3 to glutamine affects the specific interactions between the wedge loop and membrane, a sedimentation assay was performed. The result showed that PACSIN 3 P121Q did not change the binding of protein to lipid bilayers (supplemental Fig. 3*B*). Conversely, the mutations of PACSIN3 Val-122 and Leu-123 to charged residues, or deletion of them, resulted in the complete loss of the membrane binding ability even though Pro-121 is still intact (Fig. 3). These results indicate that Pro-121 is not involved in membrane insertion. Therefore, the reason that P121Q can induce the large type of tubules is not due to the change of the wedge loop insertion.

Structure-based sequence alignments also suggest that there is another residue, Glu-128 in PACSIN 3 (Glu-131 in PACSIN 1

FIGURE 3. **Tubulation and sedimentation assays of PACSIN 3 F-BAR and mutants.** *A*, negative-stained electron micrographs are shown. Liposomes were incubated with PACSIN 3 and its mutant proteins and examined by EM. ΔV122L123, V122E/L123E, V122R/L123R altered only membrane binding, whereas R127E, H119E altered only the interactions between neighboring dimers. E93R, E97R, and E100R are mutations on the contacting surface of neighboring dimer as shown in Fig. 2*C*, *left*. *B*, liposomes were incubated with PACSIN 3 and its mutant proteins and examined by sedimentation assays. Supernatant (*S*) and pellet (*P*) fractions were analyzed by SDS-PAGE. Band in pellet represents the protein bound to liposome. Histograms with means ± S.E. (*error bars*) show the quantified protein in supernatant and pellet with the total protein defined as 100%. *C*, liposomes were incubated with the His-tagged F-BAR proteins of PACSINs followed by Ni-nitrilotriacetic acid-nanogold particles (5-nm diameter) treatment and then visualized by EM.

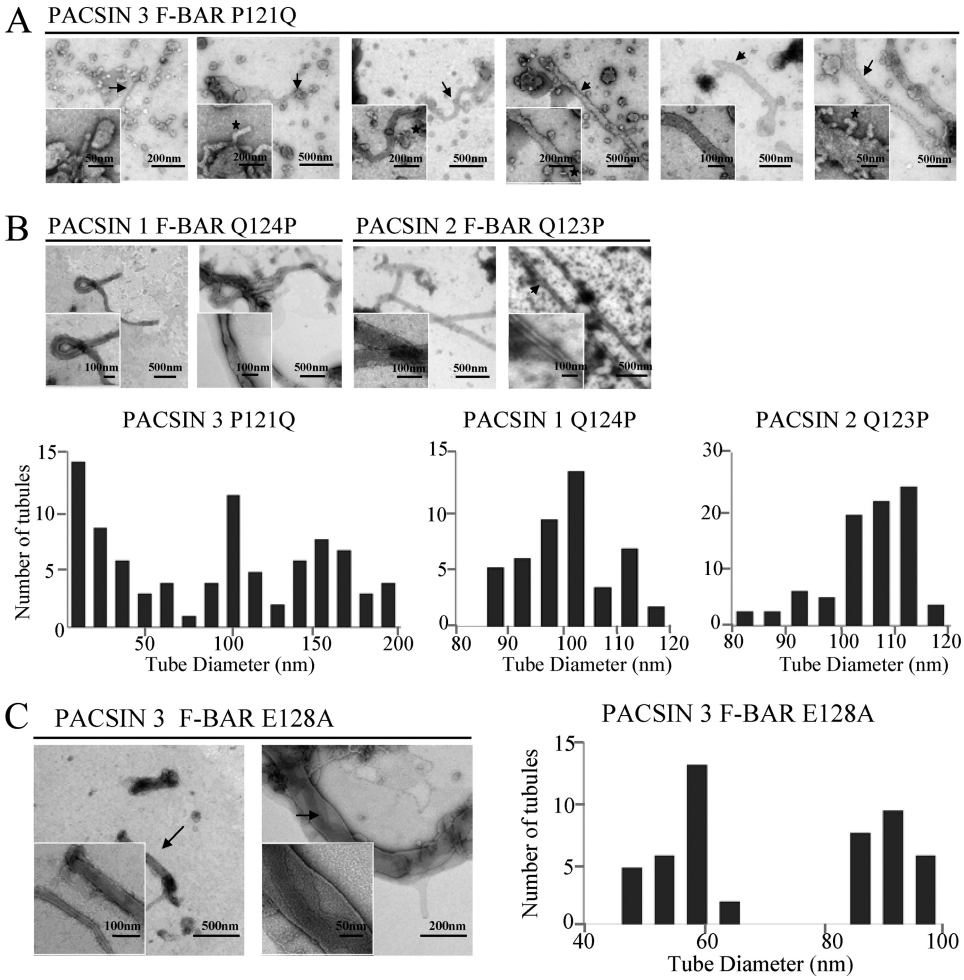

FIGURE 5. **Key residues in determination of diameter of liposome tubules.** Liposomes were incubated with different mutant proteins and examined by EM. The numbers of the tubules were quantified on five independently prepared EM grids. Membrane constrictions are denoted by *arrows*. *A*, mutation in the wedge loop of PACSIN 3 F-BAR P121Q has a profound influence on the diameters of the induced liposome tubules. *B*, substitution of residue Gln to Pro in the wedge loop of PACSIN 1 and 2 only results in low curvature tubules as shown in PACSIN 3 F-BAR in Fig. 1*C*. *C*, mutation in the wedge loop of PACSIN 3 E128A induces predominantly tubules with a diameter of 50 nm, in addition to the typical 100-nm tubules as induced by PACSIN 3 F-BAR.

and Glu-130 in PACSIN 2) that forms a hydrogen bond with the main chain of His-119 (His-122 in PACSIN 1 and His-121 in PACSIN 2) (Fig. 4*B*), may also be important for the conformation of the wedge loop. The crystal structure of the PACSIN 3 E128A mutant determined here to 2.8 Å resolution (supplemental Fig. 4 and Table 1) showed that substitution of Glu-128 with alanine eliminated the hydrogen bond between Glu-128 and His-119 (Fig. 4*B*) and resulted in a significant conformational change in the wedge loop. The E128A wedge loop of PACSIN 3 was found to resemble the wedge loop of PACSIN 1 and 2 in an outward-splayed pattern (Fig. 4*A*, *right*). Structural comparisons of the PACSIN 3 E128A loop with that of the wild type suggest that the hydrogen bond between Glu-128 and His-119 could function as a lock to maintain the loop conformation. The PACSIN 3 E128A was found to induce predominantly tubules with a diameter of 50 nm in addition to the typical 100-nm tubules induced by wild-type PACSIN3 (Fig. 5*C*), which resemble the intermediate and low curvature tubules induced by PACSIN 1 and 2. Similarly, mutants E131A and E130A of PACSIN 1 and 2 also showed more membrane constrictions budding from the tubules (supplemental Fig. 5) and more high curvature tubules compared with the wild-type PACSIN 1 and 2. These data suggest that, in PACSINs, the hydrogen bond between Glu-128 (Glu-131 or Glu-130) and His-119 (His-122 or His-121) helps to reinforce the rigidity and orientation of the wedge loop and therefore affects the curvature of the tubules.

DISCUSSION

Membrane curving by BAR domain proteins is an important biological process involved in vesicle trafficking and subcellular structure stabilization. Various tubules induced by the F-BAR domain of PACSINs are important in membrane deformation (20–25). It was suggested that the distinct wedge loop of PACSIN 1 and 2 F-BAR domains inserts into lipid bilayers of membrane (31). However, there is no clear interpretation to explain why the F-BAR domains of PACSIN 1 and 2 induce tubules with such diverse diameters.

Here, we performed structural and biochemical studies on the F-BAR domains from all three PACSINs and systematically compared the differences of the F-BAR domains between PACSIN 3 and 1, or 2 with respect to structure and membrane tubulation activities. Our analyses revealed that the more rigid wedge loop in the F-BAR domain of PACSIN 3 is responsible for its unique feature of inducing only low curvature tubules compared

with PACSIN 1 and 2. When the wedge loop in the F-BAR domain of PACSIN 1 and 2 was mutated to the more rigid structure as found in PACSIN 3, these mutants induced only low curvature tubules as the wild-type PACSIN 3. Conversely, mutants that modified the PACSIN 3 wedge loop to resemble the wedge loop in PACSIN 1 and 2 induced tubules with dimensions similar to those found in the wild-type PACSIN 1 and 2.

The distal end of murine PACSIN 2 was proposed to sense the membrane (32). Comparisons of the distal ends of wild-type PACSIN 3 with PACSIN 1 and 2 show no obvious difference in all the structures we determined (supplemental Fig. 6), suggesting that the various phenotypes presented by PACSIN 1 and 2 F-BAR may not be correlated with the intrinsic curvature of the dimer surface.

It was previously reported that during tubulation, F-BAR proteins make tip-to-tip interactions and contacts between laterally adjacent dimers (18). The diameters of the induced tubules were proposed to be related to the intrinsic large radial curvature of the F-BAR domain, such as CIP4 and FBP17 (16). However, in PACSINs, the intrinsic curvature itself certainly could not result in such diverse tubules with various diameters because PACSIN 1 and 2 induce tubules different from those induced by PACSIN 3 even though all three PACSINs almost have the same intrinsic curvature. According to the crystal packing pattern of PACSIN 3, we propose a potential membrane tubulation model for PACSINs (supplemental Fig. 7): the F-BAR domain is connected by tip-to-tip interactions and the wedge loop-mediated lateral interactions to form filaments. The filament of the F-BAR protein bends as a hinge motion at the tip-to-tip interaction to various extents. The extent of the motion is dependent on the angle between two adjacent dimers, and this angle is determined by the conformation of the wedge loop. This results in the filament winding spirally around a cylindrical membrane. The larger the angle is between the two dimers, the more the dimer bends the membrane; the more the membrane is bent, and the smaller the diameter of the tubule is (supplemental Fig. 7*E*). This model also shed light on understanding why PACSINs generate different size tubules in so many biological processes, such as trans-Golgi network vesicle formation, filopodia tips, and lamellipodia dynamics, microspike formation, and caveola fission (22, 24, 37, 38).

In conclusion, the membrane tubulation by PACSIN 3 was shown to be different from PACSIN 1 and 2, and these differences are due to different degrees of rigidity of the wedge loop. We demonstrated that the rigidity of the wedge loop in the PACSIN F-BAR domain is a key factor that determines the different angles between two neighboring dimers and dictates the diameters of various tubules. Our study provides new insights for understanding the mechanism of membrane deformation by the PACSIN family proteins.

Acknowledgments—We thank Prof. Fuyu Yang and Dr. Kai Zhao from Institute of Biophysics, Chinese Academy of Sciences, for lipid preparation; Dr. Ning Gao at Tsinghua University for the nanogold labeling assay; and Dr. Plomann at Stanford University School of Medicine for providing the PACSIN 3 plasmid. X-ray diffraction data collection was carried out at the Beijing Synchrotron Radiation Laboratory and Shanghai Synchrotron Radiation Facility.

REFERENCES

1. Merrifield, C. J., Perrais, D., and Zenisek, D. (2005) Coupling between clathrin-coated pit invagination, cortactin recruitment, and membrane scission observed in live cells. *Cell* **121,** 593–606
2. Ford, M. G., Mills, I. G., Peter, B. J., Vallis, Y., Praefcke, G. J., Evans, P. R., and McMahon, H. T. (2002) Curvature of clathrin-coated pits driven by epsin. *Nature* **419,** 361–366
3. Scott, I. C., and Stainier, D. Y. (2003) Developmental biology: twisting the body into shape. *Nature* **425,** 461–463
4. Dvorak, A. M., and Feng, D. (2001) The vesiculo-vacuolar organelle (VVO): a new endothelial cell permeability organelle. *J. Histochem. Cytochem.* **49,** 419–432
5. Rippe, B., Rosengren, B. I., Carlsson, O., and Venturoli, D. (2002) Transendothelial transport: the vesicle controversy. *J. Vasc. Res.* **39,** 375–390
6. Gallop, J. L., Jao, C. C., Kent, H. M., Butler, P. J., Evans, P. R., Langen, R., and McMahon, H. T. (2006) Mechanism of endophilin N-BAR domain-mediated membrane curvature. *EMBO J.* **25,** 2898–2910
7. Peter, B. J., Kent, H. M., Mills, I. G., Vallis, Y., Butler, P. J., Evans, P. R., and McMahon, H. T. (2004) BAR domains as sensors of membrane curvature: the amphiphysin BAR structure. *Science* **303,** 495–499
8. Itoh, T., Erdmann, K. S., Roux, A., Habermann, B., Werner, H., and De Camilli, P. (2005) Dynamin and the actin cytoskeleton cooperatively regulate plasma membrane invagination by BAR and F-BAR proteins. *Dev. Cell* **9,** 791–804
9. Bhatia, V. K., Madsen, K. L., Bolinger, P. Y., Kunding, A., Hedegård, P., Gether, U., and Stamou, D. (2009) Amphipathic motifs in BAR domains are essential for membrane curvature sensing. *EMBO J.* **28,** 3303–3314
10. Masuda, M., Takeda, S., Sone, M., Ohki, T., Mori, H., Kamioka, Y., and Mochizuki, N. (2006) Endophilin BAR domain drives membrane curvature by two newly identified structure-based mechanisms. *EMBO J.* **25,** 2889–2897
11. Takei, K., Slepnev, V. I., Haucke, V., and De Camilli, P. (1999) Functional partnership between amphiphysin and dynamin in clathrin-mediated endocytosis. *Nat. Cell Biol.* **1,** 33–39
12. Farsad, K., Ringstad, N., Takei, K., Floyd, S. R., Rose, K., and De Camilli, P. (2001) Generation of high curvature membranes mediated by direct endophilin bilayer interactions. *J. Cell Biol.* **155,** 193–200
13. Mattila, P. K., Pykäläinen, A., Saarikangas, J., Paavilainen, V. O., Vihinen, H., Jokitalo, E., and Lappalainen, P. (2007) Missing-in-metastasis and IRSp53 deform $PI(4,5)P_2$-rich membranes by an inverse BAR domain-like mechanism. *J. Cell Biol.* **176,** 953–964
14. Pykäläinen, A., Boczkowska, M., Zhao, H., Saarikangas, J., Rebowski, G., Jansen, M., Hakanen, J., Koskela, E. V., Peränen, J., Vihinen, H., Jokitalo, E., Salminen, M., Ikonen, E., Dominguez, R., and Lappalainen, P. (2011) Pinkbar is an epithelial-specific BAR domain protein that generates planar membrane structures. *Nat. Struct. Mol. Biol.* **18,** 902–907
15. Fütterer, K., and Machesky, L. M. (2007) "Wunder" F-BAR domains: going from pits to vesicles. *Cell* **129,** 655–657
16. Shimada, A., Niwa, H., Tsujita, K., Suetsugu, S., Nitta, K., Hanawa-Suetsugu, K., Akasaka, R., Nishino, Y., Toyama, M., Chen, L., Liu, Z. J., Wang, B. C., Yamamoto, M., Terada, T., Miyazawa, A., Tanaka, A., Sugano, S., Shirouzu, M., Nagayama, K., Takenawa, T., and Yokoyama, S. (2007) Curved EFC/F-BAR-domain dimers are joined end to end into a filament for membrane invagination in endocytosis. *Cell* **129,** 761–772
17. Henne, W. M., Kent, H. M., Ford, M. G., Hegde, B. G., Daumke, O., Butler, P. J., Mittal, R., Langen, R., Evans, P. R., and McMahon, H. T. (2007) Structure and analysis of FCHo2 F-BAR domain: a dimerizing and membrane recruitment module that effects membrane curvature. *Structure* **15,** 839–852
18. Frost, A., Perera, R., Roux, A., Spasov, K., Destaing, O., Egelman, E. H., De Camilli, P., and Unger, V. M. (2008) Structural basis of membrane invagination by F-BAR domains. *Cell* **132,** 807–817
19. Damke, H., Baba, T., Warnock, D. E., and Schmid, S. L. (1994) Induction of mutant dynamin specifically blocks endocytic coated vesicle formation. *J. Cell Biol.* **127,** 915–934
20. Takei, Y., Harada, A., Takeda, S., Kobayashi, K., Terada, S., Noda, T., Takahashi, T., and Hirokawa, N. (1995) Synapsin I deficiency results in the

structural change in the presynaptic terminals in the murine nervous system. *J. Cell Biol.* **131,** 1789–1800
21. Modregger, J., Ritter, B., Witter, B., Paulsson, M., and Plomann, M. (2000) All three PACSIN isoforms bind to endocytic proteins and inhibit endocytosis. *J. Cell Sci.* **113,** 4511–4521
22. Qualmann, B., and Kelly, R. B. (2000) Syndapin isoforms participate in receptor-mediated endocytosis and actin organization. *J. Cell Biol.* **148,** 1047–1062
23. Braun, A., Pinyol, R., Dahlhaus, R., Koch, D., Fonarev, P., Grant, B. D., Kessels, M. M., and Qualmann, B. (2005) EHD proteins associate with syndapin I and II and such interactions play a crucial role in endosomal recycling. *Mol. Biol. Cell* **16,** 3642–3658
24. Kessels, M. M., Dong, J., Leibig, W., Westermann, P., and Qualmann, B. (2006) Complexes of syndapin II with dynamin II promote vesicle formation at the trans-Golgi network. *J. Cell Sci.* **119,** 1504–1516
25. Grimm-Günter, E. M., Milbrandt, M., Merkl, B., Paulsson, M., and Plomann, M. (2008) PACSIN proteins bind tubulin and promote microtubule assembly. *Exp. Cell Res.* **314,** 1991–2003
26. Halbach, A., Mörgelin, M., Baumgarten, M., Milbrandt, M., Paulsson, M., and Plomann, M. (2007) PACSIN 1 forms tetramers via its N-terminal F-BAR domain. *FEBS J.* **274,** 773–782
27. Plomann, M., Lange, R., Vopper, G., Cremer, H., Heinlein, U. A., Scheff, S., Baldwin, S. A., Leitges, M., Cramer, M., Paulsson, M., and Barthels, D. (1998) PACSIN, a brain protein that is up-regulated upon differentiation into neuronal cells. *Eur. J. Biochem.* **256,** 201–211
28. Ritter, B., Modregger, J., Paulsson, M., and Plomann, M. (1999) PACSIN 2, a novel member of the PACSIN family of cytoplasmic adapter proteins. *FEBS Lett.* **454,** 356–362
29. Rao, Y., Ma, Q., Vahedi-Faridi, A., Sundborger, A., Pechstein, A., Puchkov, D., Luo, L., Shupliakov, O., Saenger, W., and Haucke, V. (2010) Molecular basis for SH3 domain regulation of F-BAR-mediated membrane deformation. *Proc. Natl. Acad. Sci. U.S.A.* **107,** 8213–8218
30. Qualmann, B., Roos, J., DiGregorio, P. J., and Kelly, R. B. (1999) Syndapin I, a synaptic dynamin-binding protein that associates with the neural Wiskott-Aldrich syndrome protein. *Mol. Biol. Cell* **10,** 501–513
31. Wang, Q., Navarro, M. V., Peng, G., Molinelli, E., Goh, S. L., Judson, B. L., Rajashankar, K. R., and Sondermann, H. (2009) Molecular mechanism of membrane constriction and tubulation mediated by the F-BAR protein PACSIN/syndapin. *Proc. Natl. Acad. Sci. U.S.A.* **106,** 12700–12705
32. Plomann, M., Wittmann, J. G., and Rudolph, M. G. (2010) A hinge in the distal end of the PACSIN 2 F-BAR domain may contribute to membrane-curvature sensing. *J. Mol. Biol.* **400,** 129–136
33. Bai, X., Meng, G., Li, G., Luo, M., and Zheng, X. (2010) Crystallization and preliminary x-ray crystallographic analysis of human PACSIN 1 protein. *Acta Crystallogr. Sect. F Struct. Biol. Cryst. Commun.* **66,** 73–75
34. Collaborative Computational Project, Number 4 (1994) The CCP4 suite: programs for protein crystallography. *Acta Crystallogr. D Biol. Crystallogr.* **50,** 760–763
35. Powell, H. R. (1999) The Rossmann Fourier autoindexing algorithm in MOSFLM. *Acta Crystallogr. D Biol. Crystallogr.* **55,** 1690–1695
36. Emsley, P., and Cowtan, K. (2004) COOT: model-building tools for molecular graphics. *Acta Crystallogr. D Biol. Crystallogr.* **60,** 2126–2132
37. Senju, Y., Itoh, Y., Takano, K., Hamada, S., and Suetsugu, S. (2011) Essential role of PACSIN2/syndapin-II in caveolae membrane sculpting. *J. Cell Sci.* **124,** 2032–2040
38. Shimada, A., Takano, K., Shirouzu, M., Hanawa-Suetsugu, K., Terada, T., Toyooka, K., Umehara, T., Yamamoto, M., Yokoyama, S., and Suetsugu, S. (2010) Mapping of the basic amino acid residues responsible for tubulation and cellular protrusion by the EFC/F-BAR domain of PACSIN2/syndapin II. *FEBS Lett.* **584,** 1111–1118